

Supporting information for

Light Emission as a Probe of Energy Losses in Molecular Junctions

Oleksii Ivashenko¹, Adam J. Bergren^{2*} and Richard L. McCreery^{1,2*}

¹University of Alberta, 11421 Saskatchewan Dr., Edmonton, AB T6G 2M9, Canada

²National Institute for Nanotechnology, 11421 Saskatchewan Dr., Edmonton, AB T6G 2M9, Canada

Table of contents

1.	Experimental setup.....	2
2.	$h\nu_{co}$ determination.....	3
3.	Sample preparation	3
4.	Additional light emission spectra.....	6
5.	Top contact variation	8
6.	Yield information.....	8
7.	Spectra correction	9
8.	Comparison with a black body radiation	11

1. Experimental setup

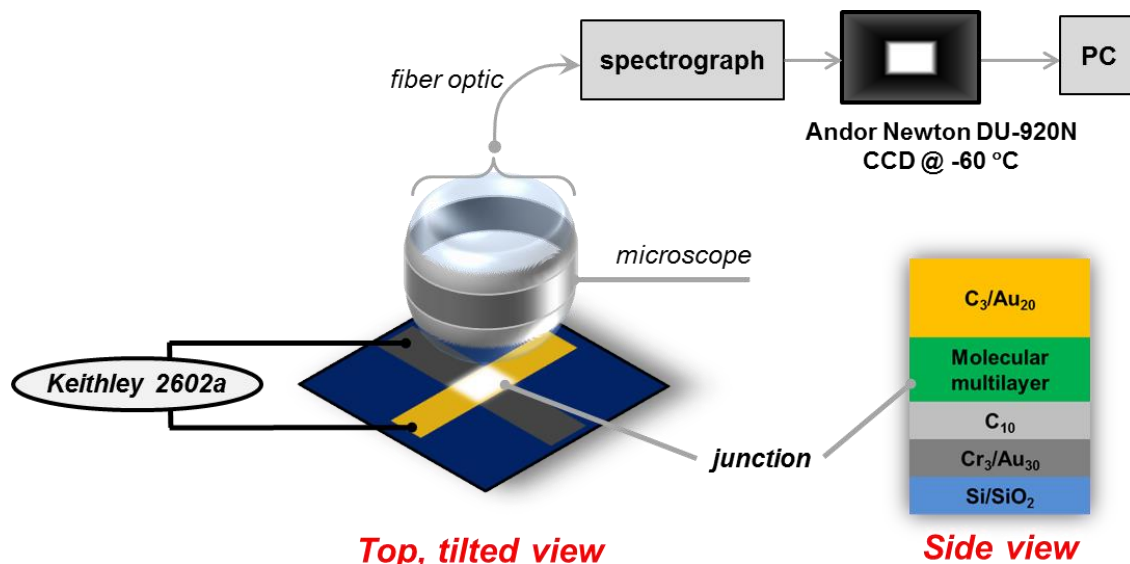


Figure SI 1. Schematic of the experimental setup used for light emission measurements. A crossed junction was biased with DC (Keithley 2602A) voltage resulting in light emission. Light was collected using a 50x objective (numerical aperture = 0.45) on an Olympus BX-60 microscope with a fiber optic output, delivering the light to an Andor Shamrock spectrograph equipped with an Andor Newton DU-920N CCD detector, cooled to -60 °C.

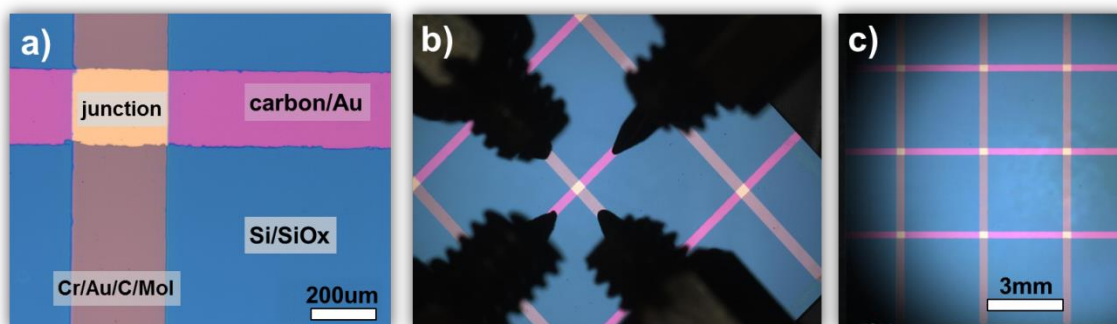


Figure SI 2. Optical images of the junction. a) Labeled photograph of a molecular junction on a Si/SiO_x substrate, with Cr/Au/eC bottom contact with a covalently grafted molecular layer, and carbon/Au top contact. b) Molecular junction mounted into the sample holder with four probes to apply electrical bias for light emission measurements. c) Larger scale image of the chip consisting of 12 junctions (only 9 are visible).

The experimental setup for light emission measurements consisted of an Olympus BX60 microscope stage and fiber optic output coupled to an Andor Solis spectrograph with an Andor Newton DU-920N CCD cooled to -60 °C. Samples were mounted on a custom-built sample holder with 4 probes for applying an external bias using a Keithley 2602a in a DC mode. A Keithley 2602a was connected to the sample stage throughout the experiment, *i.e.* for initial and final *i-V* curve measurements as well as for DC bias application.

After electrical connection, samples were aligned in the microscope stage and focused using a 50x objective (where the field of view was approximately the same as the junction area) and an *i-V* curve was acquired with a Keithley 2602a to verify contact and ensure a non-shortcd sample. An opaque screen was used to isolate the stage from external ambient background light.

Acquisition of light consisted of the measurement of a background with no bias applied to the sample, with subsequent spectral collection starting at low initial bias values to verify the absence of emission at $V_{app} < V_{onset}$. Spectra were measured using 4 accumulations of 7.5 s with a 50 kHz readout rate, a preamplifier gain of 4x, full vertical binning, and 8 pixel horizontal binning. Intermediate measurements of i - V curves were conducted to verify sample function.

2. $h\nu_{co}$ determination

Further analysis of the spectra consisted of intensity evaluation and $h\nu_{co}$ determination on raw, uncorrected spectra. $h\nu_{co}$ determination was performed by calculating the point where two lines cross: 1) a 3σ line representing the detection limit for light; and 2) a linear fit for each spectrum in the range of 3σ to 10σ on the high-energy side of the spectrum. There are several errors contributing to the uncertainty of $h\nu_{co}$ determination by this method. The fitting error is ± 0.1 eV and the calibration error ± 0.05 eV. Additionally, after correction for a spectrometer response curve, emission spectra shift ~ 0.1 eV to the lower energy. Therefore the overall uncertainty in the $h\nu_{co}$ determination obtained in this method is ± 0.2 eV.

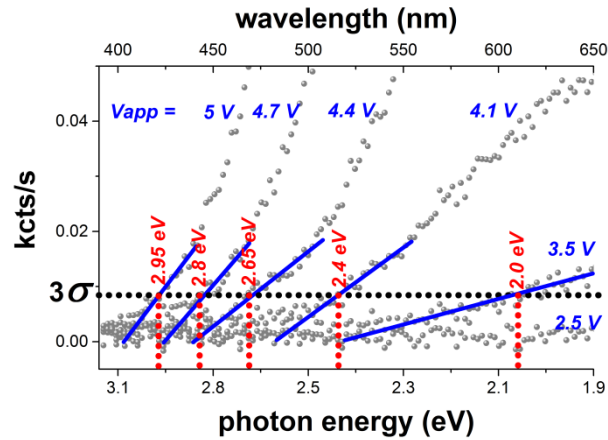


Figure SI 3. An example of linear fit (blue solid lines) of the high energy range of the light emission spectrum (enlarged part of the light emission spectrum) for Si/SiO_{x300}/Cr₄/Au₃₀/eC₁₀/NAB₈/eC₃/Au₂₀, which was used to determine cut off values (shown in red) at the intensity level of 3σ (black dotted line).

3. Sample preparation

NDI, NAB, AB diazonium salts were synthesized as previously reported by diazotization of the aromatic amine precursor^{1,2}. BTB aromatic amine precursor was obtained from the laboratory of Jean-Christophe Lacroix at the University of Paris, where it was synthesized as described previously³. Its diazonium ion was prepared in situ as described below.

AlOx junction preparation. Cross-junctions with a typical area of 0.014 cm^2 were prepared on Si (Ei-Cat Inc.) chips ($1.85 \times 1.3 \text{ cm}$) with 320–340 nm of wet thermal silicon oxide grown on the surface as an insulating layer using the University of Alberta Nanofab Minibrute furnace. Substrates were cleaned by sonication in acetone, isopropanol and water for 20 min in each solvent, and then dried with a stream of N₂ and loaded into an electron beam evaporation system for bottom contact deposition. Evaporation of

3 nm chromium (99.998%, Kurt J. Lesker) at a 1 Å/s rate was used for an adhesion layer, followed by evaporation of 40 nm of aluminum (99.99%, Alfa Aesar) at 3 Å/s rate (back pressure during deposition was $2-5 \times 10^{-6}$ Torr). The aluminum was oxidized by heating the sample to ca. 200° C for 10 min in air. After oxidation, which yielded ~4 nm AlOx (estimated by XPS), the sample was loaded into an electron beam evaporation system for top contact deposition. 30 nm Au (99.99%, MRCS Canada) was deposited at 3 Å/s through a shadow mask oriented perpendicular to the Al contact, resulting in a cross junction. The roughness of a typical AlOx junction surface was estimated by tapping mode atomic force microscopy (AFM), which gave RMS values of 3.5 ± 0.5 nm. The final composition of the junction was Si/SiO_{x320}/Cr₃/Al₄₀/AlO_{x4}/Au₃₀.

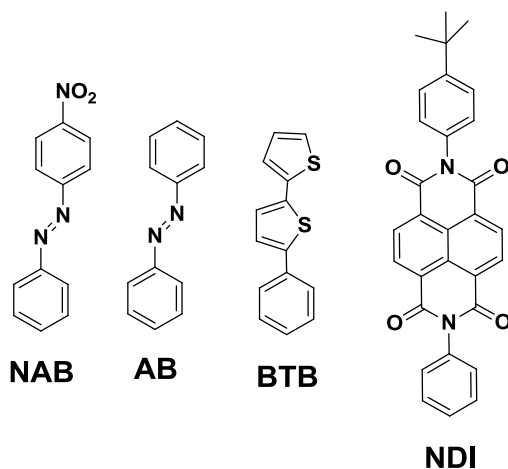


Figure SI 4. Molecular structures of the monomers used to prepare molecular films: nitroazobenzene (**NAB**), azobenzene (**AB**), bithienylbenzene (**BTB**) and naphthalene di-imide derivative (**NDI**). In all cases aromatic amine precursors with para NH₂ group on the bottom phenyl ring of the molecules shown was converted to a diazonium ion before deposition on the eC substrate.

Molecular junction preparation. Fabrication of large area (0.00068 cm²) molecular junctions with the structure Si/SiO_x/Cr/Au/eC/Mol/eC/Au consisted of 3 steps: 1) preparation of a bottom contact by evaporation of Cr/Au/eC on a Si/SiO_x substrate; 2) grafting of molecular layer; 3) evaporation of the top contact consisting of C/Au.

Si/SiO₂ diced wafer chips (1.85×1.3 cm) with 320-340 nm silicon oxide layer were cleaned by sonication in acetone, isopropanol and water for 20 min in each solvent and dried with a stream of N₂ before loading into the electron beam deposition system.

1) The bottom contact was deposited by consecutive evaporation of 3 nm Cr (99.998%, Kurt J. Lesker) at 0.2 Å/s rate; 30 nm of Au (99.99%, MRCS Canada) at 0.2 Å/s rate; and 10 nm C (2spi.com) at a rate of 0.2 Å/s in a Johnson Ultravac e-beam evaporator at a base pressure $< 2 \times 10^{-6}$ Torr. Four vertical lines on a chip were prepared through a shadow mask in this way and to serve as the substrate for step 2 (electrochemical grafting of the molecular layer). The RMS roughness of the bottom contact was 0.6 ± 0.1 nm, as determined by AFM.

2) Preparation of a multilayer molecular film was conducted using the electrochemical reduction of diazonium salts of several molecules: nitroazobenzene (**NAB**), azobenzene (**AB**), and a naphthalene di-imide derivative (**NDI**). Grafting was performed using a CH Instruments potentiostat with a three electrode compartment. Si/SiO_x/Cr/Au/eC electrodes prepared in step 1 were used as a working electrode, with a Pt wire auxiliary and Ag/AgCl reference electrodes. The solution for grafting consisted of 1mM diazonium salt precursor (**NAB**, **AB**, **NDI**) with 0.1 M tetrabutylammonium tetrafluoroborate supporting electrolyte in acetonitrile. The solution was purged with high-purity Ar gas for 20 min prior to electrochemical scanning. Freshly evaporated bottom electrodes were used immediately after removal from the deposition system for functionalization. Table 1 contains experimental conditions used to grow

molecular films. After grafting, substrates were carefully rinsed with acetonitrile, dried with a stream of N₂, and introduced into the electron beam system for evaporation of the top contact, step 3. Preparation of films of **BTB** was done as described previously⁴ under experimental conditions listed in table 1.

Table SI 1. Grafting parameters for **NAB**, **AB**, **NDI** and **BTB** molecular layers.

Molecule	Thickness (nm)	Starting potential (V)	Maximum negative potential (V)	Scan rate (V s ⁻¹)	Number of cycles
NAB	5.4±0.4	0.4	-0.45	0.2	4
	6.1±0.4	0.4	-0.5	0.2	5
	8±0.5	0.4	-0.75	0.2	8
	10.1±0.5	0.4	-0.9	0.2	8
	16.2±0.5	0.4	-1.0	0.2	8
	19.3±0.6	0.4	-1.05	0.2	8
AB	7.0±0.4	0.4	-0.9	0.2	8
NDI	7.9±0.5	0.3	-0.6	0.05	10
BTB	7.0±0.3	0.4	-0.4	0.1	2
	10.2 ±0.4	0.4	-0.4	0.1	4
	13.4±0.5	0.4	-0.6	0.1	4
	21.0±0.6	0.4	-0.6	0.1	10

3) C_{3nm}/Au_{20nm} was evaporated at 0.2 Å/s rate at a pressure <2×10⁻⁶ mbar was deposited horizontally across the substrate lines as the top contact. Completed junctions were removed from the vacuum chamber and stored in air for 12 h before light emission measurements.

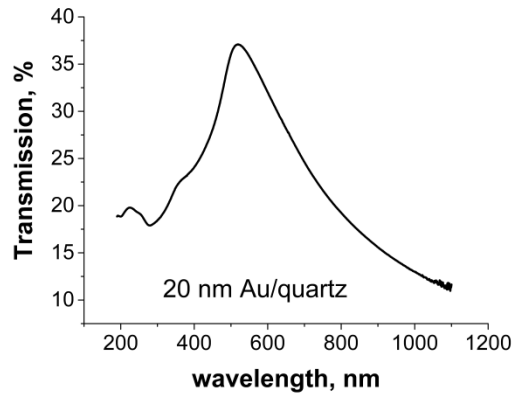


Figure SI 5. Transmission spectrum of 20 nm of Au on quartz, representative of the light transparency of the top contact for molecular junctions. Attenuation of photons by the top contact will depend on the site of light emission as well as plasmon damping by the e-Carbon layer.

Thickness measurements were obtained using atomic force microscopy (AFM) using a DI-NANOMAN 3100. SPM probes from MikroMasch with a resonance frequency of ~325 kHz and spring constant of ~40 N/m were used for the measurements. A 1×1 μm area of the sample SiO_x/Cr/Au/eC/NAB immediately adjacent to the junction used for light emission was “scratched” in a contact AFM mode with amplitude setpoint of 0.5 V to create a trench⁵. A subsequent 5×5 μm image collected in tapping mode was analyzed to determine molecular layer thickness by using Gaussian fits to height histograms of the

image with the mean difference between height of molecular surface and underlying substrate surface, with a typical measurement error of ± 0.5 nm⁶.

4. Additional light emission spectra

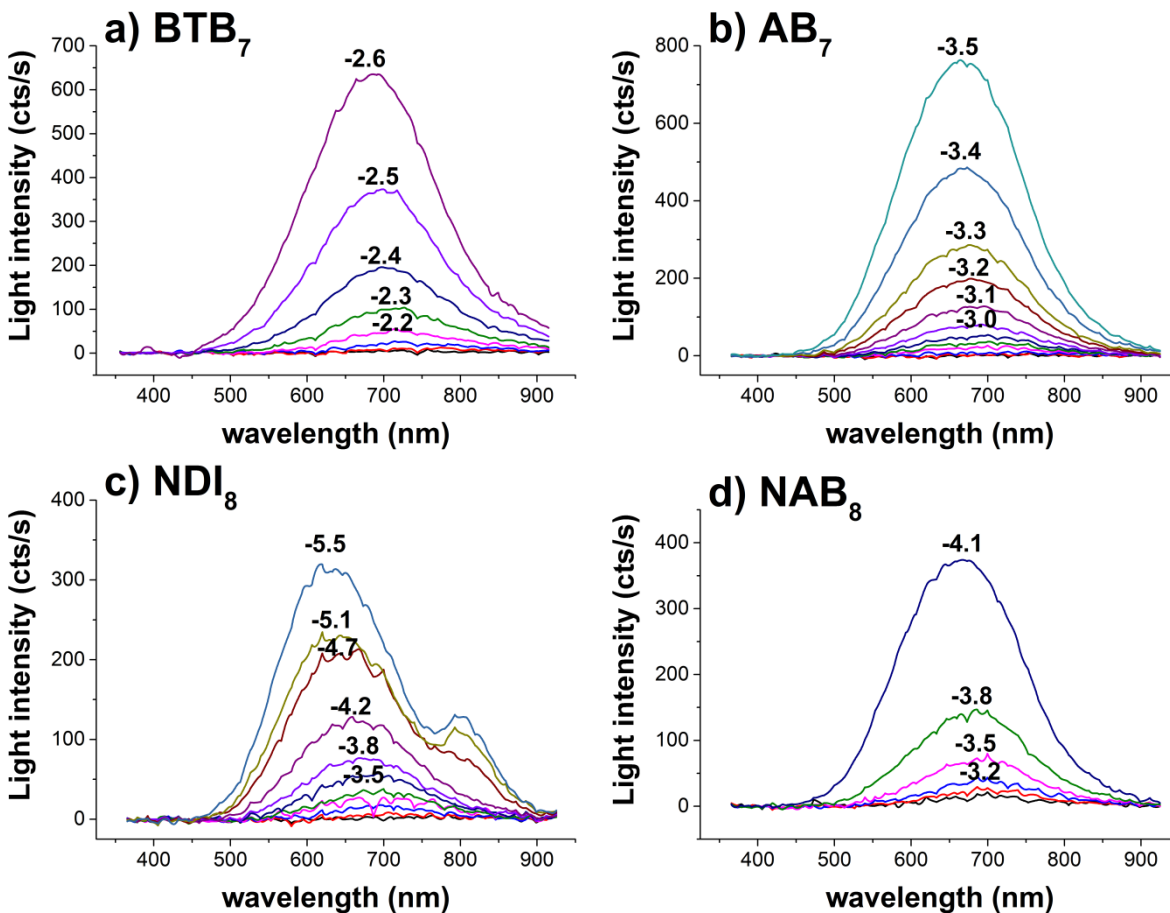


Figure SI 6. Light emission spectra for several structurally different junctions (mol₇₋₈/eC₃/Au₂₀) with similar thickness of 7-8 nm: a) BTB₇; b) AB₇; c) NDI₈; d) NAB₈. NDI shows an additional feature at ca. 800 nm which was attributed to electroluminescence from the NDI unit.

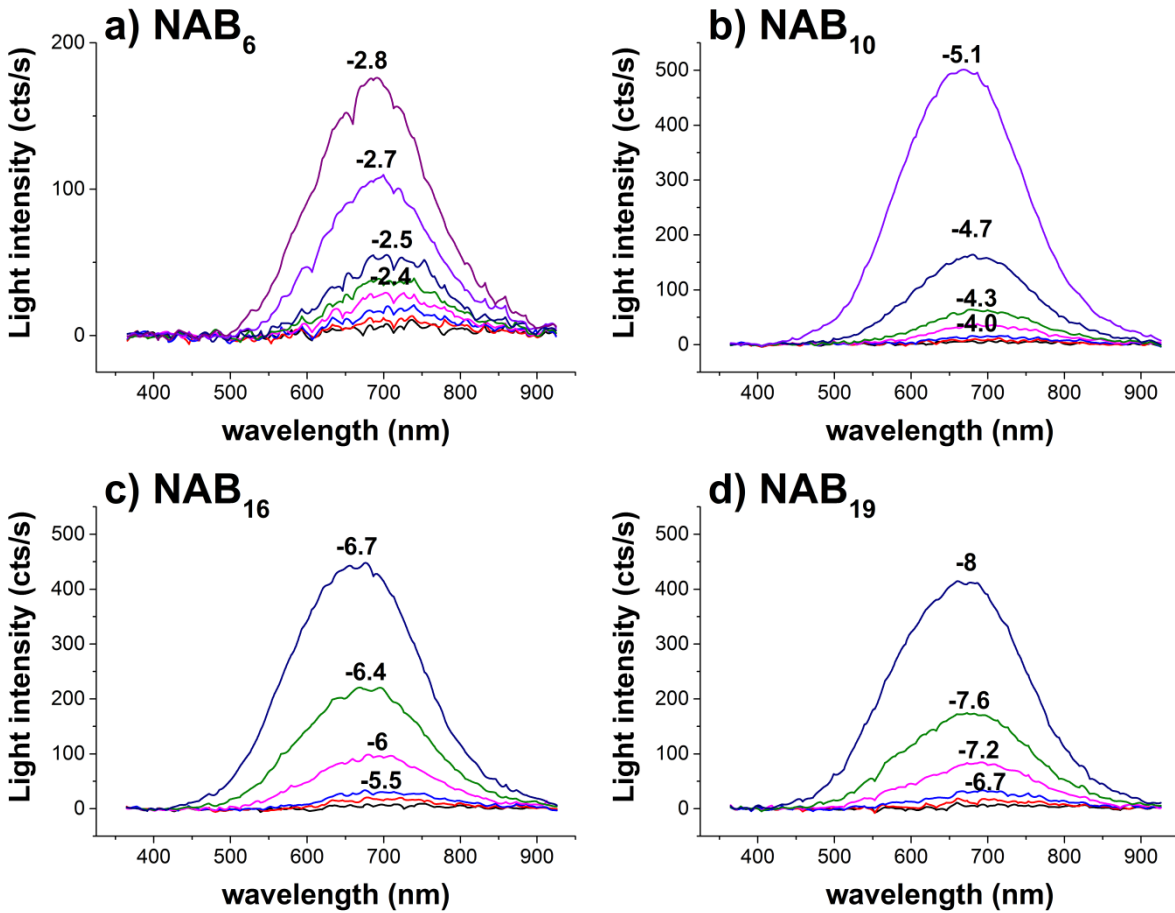


Figure SI 7. Light emission spectra for NAB/eC₃/Au₂₀ junctions with variable thickness 6-19 nm.

5. Top contact variation

All of the molecular junctions reported in the main text (except for Al/AIOx/Au) had the same device structure, i.e. Au₃₀/eC₁₀/molecule/eC₃/Au₂₀, with the molecular layer thickness varying from 4 to 22 nm. However, since the composition and plasmonic properties of the contacts affect the emission spectrum, alternative device structures were examined for their effects on $h\nu_{co}$ and energy losses. Results for Au₃₀/eC₁₃/NAB₈ devices with four different top contacts are shown in figure SI 8. The addition of the eC₃ layer significantly increased the fabrication yield compared to Au- and Cu-only top contacts, but also decreased the emitted intensity (8c). The emission spectrum is affected by top contact composition (8b), but plots of $h\nu_{co}$ vs. V_{app} were all linear with similar slopes (8d). The offset in the X-axis of the JV and $h\nu_{co}$ plots is small compared to the total energy losses, and might be due to differing work functions of the top contacts.

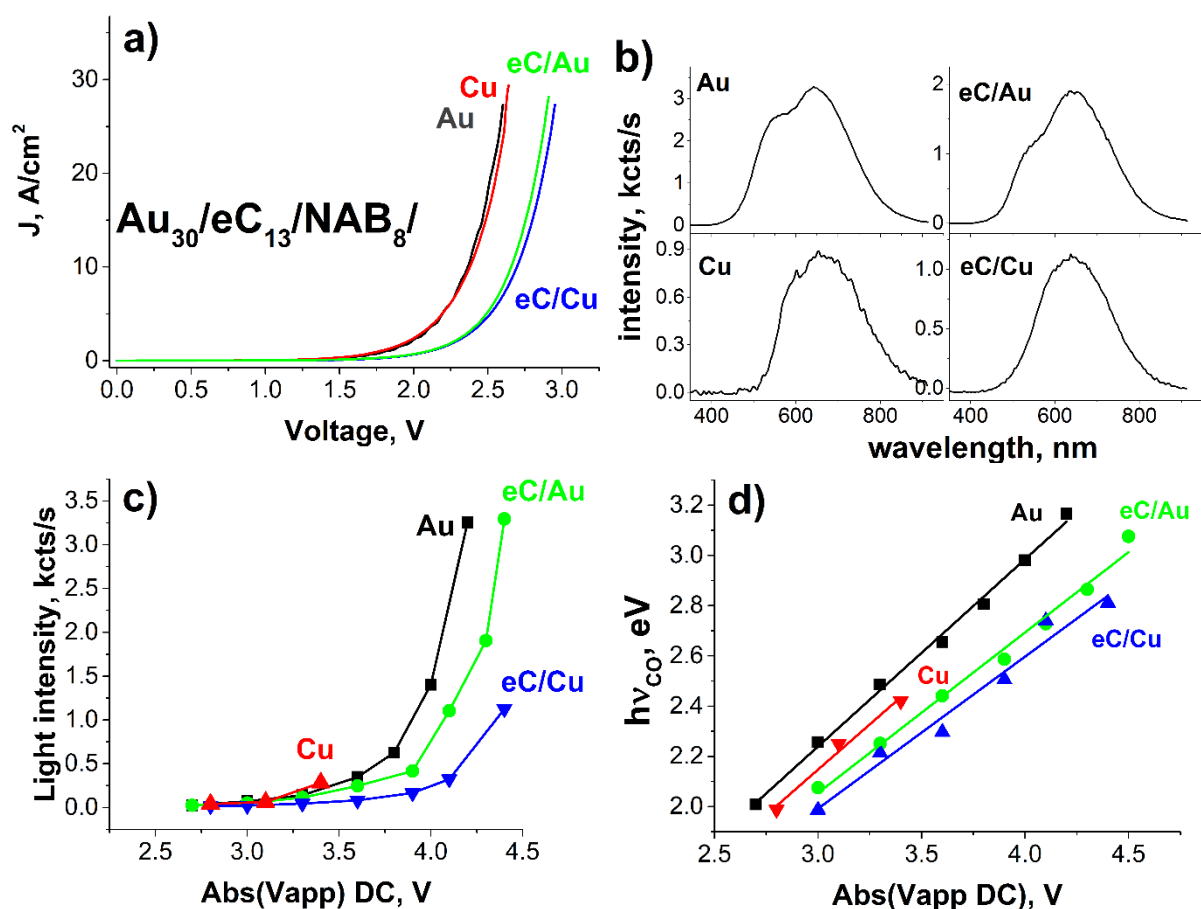


Figure SI 8. a) J-V curves of molecular junctions Au₃₀/eC₁₃/NAB₈/ with top contacts made of Au₃₀, eC₃/Au₃₀, Cu₃₀, eC₃/Cu₃₀. b) Corresponding light emission spectra of the same molecular junctions measured at Abs(V_{app} DC) = 4.3 V. Junction with Cu contact was measured separately in AC mode at V_{app} = 3.8 V. c) Light emission intensity for the same junctions measured in DC mode for a range of applied biases. d) Cutoff values for the same junctions measured in DC mode for a range of applied biases.

6. Yield information

Multiple (12) batches of molecular junctions were studied with the aim to have the most complete and informative dataset including thickness range up to 19 nm and several molecular structures. Each

batch of samples consisted of minimum 6 chips, each with 12 junctions. Four batches are presented in this paper are related to NAB, BTB, NDI, AB with thickness variation 5-19 nm. In most cases reported, the light emission results were obtained from the same junctions that exhibited the JV response of figure 1 in the main text.

Table SI 2. Yield and reproducibility for electronic and light emission measurements

Molecular junction	Production yield* #/total per chip	Yield suitable for LE** #/total	RSD of current for junctions suitable for LE at $J = -30 \text{ A/cm}^2, \text{ A/cm}^2$	Number of J tested for light emission
NAB ₅	3/4	3/4	1.5 (5%)	1
NAB ₆	9/12	2/12	0.3 (1%)	1
NAB ₁₀	4/8	4/8	5 (17%)	1
NAB ₁₆	4/4	4/4	5.1 (17%)	1
NAB ₁₉	4/4	4/4	3.8 (13%)	1
NAB ₈	6/8	4/8	2.7 (9%)	3
NDI ₈	8/8	4/8	6.8 (23%)	4
BTB ₇	5/5	3/5	3.6 (12%)	2
AB ₇	12/12	9/12	4.3 (14.5%)	2

*Production yield - % of not shorted junctions of the same thickness.

**Yield suitable for light emission - % of junctions that can tolerate current density of 30 A/cm^2 .

7. Spectra correction

In order to account for the variable sensitivity of the CCD detector in the range 200-1050 nm (Figure SI 9), a correction for the spectrometer response function was carried out using a calibrated light source (Ocean Optics LS-1-CAL) to determine a transmission (collection) function that could be applied to selected raw spectra obtained from devices. The main motivation for this procedure were to obtain the real emission spectrum of the light emission and subsequently to compare it with simulated emission of black body radiation, as shown in section 7 below.

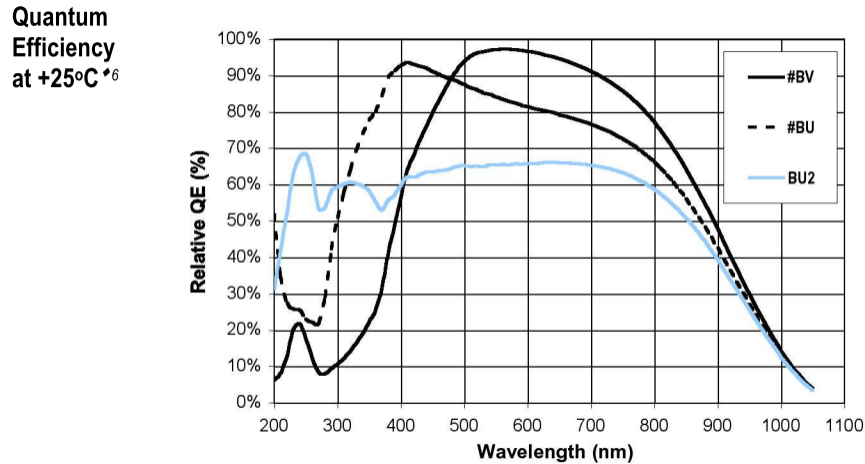


Figure SI 9. Quantum efficiency curve for Andor Newton CCD DU-920N BU camera used in the measurements showing high sensitivity in the visible-NIR region 300–900 nm.

A calibrated light source with a known power density (I^{S0}) was directed onto a diffuse reflectance Teflon standard surface (Ocean Optics WS-1) and spectra acquired using the same acquisition parameters used for the measurements of NAB junctions – four 7.5 s accumulations, 50 kHz readout rate, preamplifier gain 4x, full vertical binning, and horizontal binning of 8 pixels. The collection function was obtained according to the equation:

$$I^S(\lambda) = C(\lambda) \times I^{S0}(\lambda), \quad (1)$$

where $I^S(\lambda)$ is the observed intensity at wavelength λ , $I^{S0}(\lambda)$ is the light intensity of the calibrated source at the same wavelength, and $C(\lambda)$ is corresponding collection function, with I^S measured through the same optical system as the MJ light emission spectrum, including CCD, fiber optics and focusing system. Obtained $C(\lambda)$ was used to correct the raw spectra of NAB according to the equation:

$$I_0^{\text{NAB}}(\lambda) = \frac{I_{\text{raw}}^{\text{NAB}}(\lambda)}{C(\lambda)}, \quad (2)$$

where $I_0^{\text{NAB}}(\lambda)$ is the corrected intensity at wavelength λ , $I_{\text{raw}}^{\text{NAB}}(\lambda)$ is the raw light emission intensity at the same wavelength, and $C(\lambda)$ is the corresponding collection function found in (1).

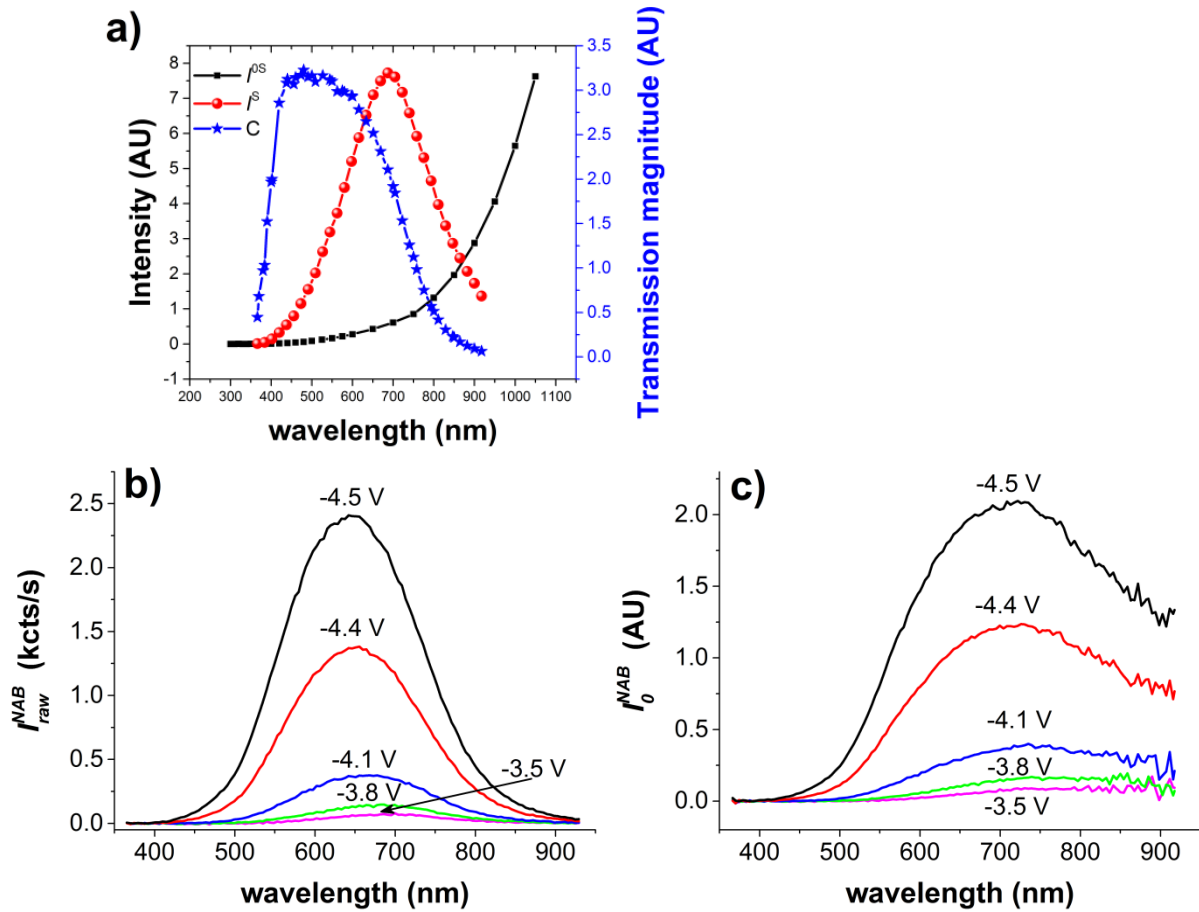


Figure SI 10. a) Calibrated output from the standard light source I^{S0} (black line with squares), measured spectrum I^S (red line with spheres) and spectrometer collection function C (blue line with stars). b) Raw $I_{\text{raw}}^{\text{NAB}}$ and c) corrected I_0^{NAB} spectrum of NAB/eC/Au junction measured at variable negative bias.

A typical uncorrected spectrum of NAB/eC/Au shows an emission peak centered at 656 nm, which broadens after correction and shifts to ~725 nm. The corrected spectrum contains more noise above 800 nm due to reduced detector quantum efficiency, and it is difficult to establish the low energy emission onset above 900 nm. However, it is possible to conclude that emission is decreasing in the near IR range.

The corrected spectra are used below to investigate the possibility of Joule-heating-induced black body radiation contributing to light emission in molecular devices.

8. Comparison with a black body radiation

The possibility that light emission from molecular junctions is due to black body radiation was considered, by comparing predicted black body radiation for several temperatures to the corrected molecular junction output, as shown in Figure SI 11. Since black body radiation depends only on temperature and not on identity of material, emission from junctions with Au and Cu should be identical if observed at similar temperatures. However, our experimental data (in preparation for the following, more detailed report) shows that for a given applied bias, the light emission spectra for junctions with Au and Cu top contact exhibit distinct shapes. These results imply that Joule heating is not a significant contribution to the experimental spectra in Figure 2 in the main text.

Further indications that Joule heating is unlikely to explain the results can be derived considering the junction temperature and the nature of spectral parameters such as $h\nu_{c_0}$ that are required to observe spectra like those in Figure 2. At room temperature and below 800 K no light in the visible region can be observed from a black body (Figure SI 11). As the temperature increases, λ_{max} progressively shifts towards the visible region, reaching 700 nm (typical λ_{max} for NAB molecular junctions) at 4150 K. Further analysis of spectra for black body hotter than 2000 K shows that no peak in the spectra for black body radiation is expected in the visible region until the temperature exceeds 4150 K. Such temperatures would obviously destroy the device, so there is no evidence that black body radiation contributes significantly to the observed light emission.

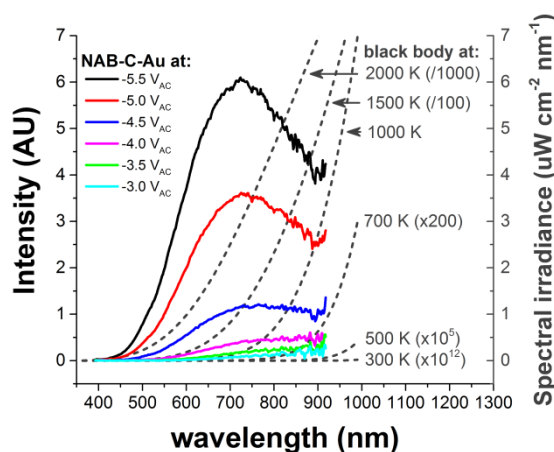


Figure SI 11. Overlay of corrected light emission spectra for Si/SiO_{x300}/Cr₄/Au₃₀/eC₁₀/NAB_{7.4}/eC₃/Au₂₀ measured in negative polarity (colored solid lines, left Y axis) and simulated black body radiation spectra (grey dashed lines, right Y axis) for several temperatures below 2000 K. Black body spectra were rescaled accordingly to facilitate better comparison.

References

- (1) Solak, A. O.; Eichorst, L. R.; Clark, W. J.; McCreery, R. L. *Anal. Chem.* **2003**, *75*, 296.
- (2) Liu, Y.-C.; McCreery, R. L. *J. Am. Chem. Soc.* **1995**, *117*, 11254.
- (3) Fave, C.; Leroux, Y.; Trippe, G.; Randriamahazaka, H.; Noel, V.; Lacroix, J.-C. *Journal of the American Chemical Society* **2007**, *129*, 1890.

- (4) Yan, H.; Bergren, A.; McCreery, R.; Della Rocca, M.; Martin, P.; Lafarge, P.; Lacroix, J. *Proceedings of the National Academy of Sciences of the United States of America* **2013**, *110*, 5326.
- (5) Anariba, F.; DuVall, S. H.; McCreery, R. L. *Anal. Chem.* **2003**, *75*, 3837.
- (6) Sayed, S. Y.; Fereiro, J. A.; Yan, H.; McCreery, R. L.; Bergren, A. J. *Proceedings of the National Academy of Sciences of the United States of America* **2012**, *109*, 11498.